

# Jump Conditions and Surface-Excess Quantities at a Fluid/Porous Interface: A Multi-scale Approach

M. Chandesris · D. Jamet

Received: 20 November 2007 / Accepted: 20 October 2008 / Published online: 14 November 2008  
© Springer Science+Business Media B.V. 2008

**Abstract** We present a two-step up-scaling approach that allows to derive the jump conditions that must be imposed at the interface to account for transport phenomena in a fluid/porous domain. This general approach is first applied to a heat conduction problem to illustrate the main steps of the analysis. The heat flux and temperature jump conditions are related to surface-excess quantities, whose values depend on the interface location. Good agreement between the mesoscopic and macroscopic results are obtained, whatever the position of the interface inside the transition region. The approach is then applied to the problem of a laminar flow over a porous medium. The Beavers and Joseph relation is recovered, but only for a particular position of the interface.

**Keywords** Interface · Jump conditions · Excess quantity · Multi-scale

## 1 Introduction

For the study of practical applications involving flows and heat transfer over porous media, the most commonly used modeling approach is to consider two homogeneous regions (a free fluid region and a porous region) separated by a discontinuous interface. To connect the transport models used in each region, appropriate boundary conditions need to be specified at this interface. The determination of these boundary conditions is the subject of many different contributions, the most famous being the semi-empirical relation introduced by [Beavers and Joseph \(1967\)](#) to model the momentum transfer for a Poiseuille flow over a porous medium:

$$\left. \frac{du}{dy} \right|_+ = \frac{\alpha}{\sqrt{K_p}} (u_B - U_D) \quad (1)$$

---

M. Chandesris (✉) · D. Jamet  
CEA, DEN, Département d'Etudes des Réacteurs, CEA/Grenoble, DEN/DER/SSTH, 17 Rue des Martyrs,  
38054, Grenoble Cedex 9, France  
e-mail: marion.chandesris@cea.fr

D. Jamet  
e-mail: didier.jamet@cea.fr

Here,  $u$  is the velocity in the direction tangential to the interface,  $K_p$  is the permeability of the porous medium,  $U_D$  is the Darcy velocity in the porous medium,  $u_B$  is the slip velocity at the interface and  $\alpha$  is a dimensionless jump coefficient. This relation allows to take into account the non-zero velocity that develops at the permeable wall. Regarding the jump coefficient  $\alpha$ , many studies have focused on the determination of its value (Taylor 1971; Beavers et al. 1974; James and Davis 2001). It depends strongly on the geometry of the transition region but also on the exact location of the interface (Larson and Higdon 1986, 1987; Sahraoui and Kaviani 1992; Saffman 1971; Saleh et al. 1993). However, no agreement on a best choice for the exact location of the interface inside the transition region has been reached.

This ambiguity concerning the localization of the interface is representative of the confusion that exists between the different scales of description of the fluid/porous interface, the different models associated to these scales and the way these models are derived. This confusion arises because one needs to connect two domains that are commonly treated using two different approaches: in the free fluid domain, the flow is modeled using the Navier–Stokes equations and is therefore represented at a microscopic scale, whereas in the porous domain, the flow is represented using a macroscopic model (e.g., Darcy, Forchheimer, Darcy–Brinkman equations). The difficulty is thus to connect these two domains, which are modeled using different scales of description, in a way that takes into account the transfers at the fluid/porous interface.

To deal with this difficulty, Ochoa-Tapia and Whitaker (1995) introduce the idea of *deriving* these boundary conditions, starting from the knowledge of the flow at the microscopic scale and using up-scaling methods. They obtain a stress jump boundary condition that is widely used (e.g. Kuznetsov 1997; Breugem et al. 2005). However, this jump condition still depends on an unknown parameter which depends on the exact location of the interface. Following their up-scaling idea, Chandesris and Jamet (2006) developed a two-step up-scaling methodology based on three different levels of description of the interface (Fig. 1). The introduction of these three levels of description is very important to dissociate the different steps of the interface modeling process, to identify the characteristic length scales associated to each level and to clarify the hypotheses and concepts associated to each scale of description.

First, we present this multi-scale approach from a general point of view in Sect. 2. To illustrate how this method can be applied to study transport phenomena at a fluid/porous interface, a heat conduction problem is studied in Sect. 3. In the last part, Sect. 4, we come back to the empirical slip boundary condition of Beavers and Joseph (1) and show how it can be recovered from the results of this multi-scale approach.

## 2 Modeling Approach

### 2.1 First Up-scaling Step

When studying physical phenomena in hybrid fluid/porous domains, the flow in the porous domain is represented using a macroscopic model. This macroscopic description is obtained after an up-scaling step, which can be performed using the volume averaging method (Whitaker 1999). To solve the modeling difficulty in the vicinity of the interface region, the idea is to apply the averaging volume of size  $r_0$  not only in the porous region but also in the *entire* domain and in particular across the interfacial region. Thus, the *same* averaging volume is used in the whole domain. After such a volume averaging procedure, the vicinity of the interface region is a *continuous transition region* across which all the physical variables

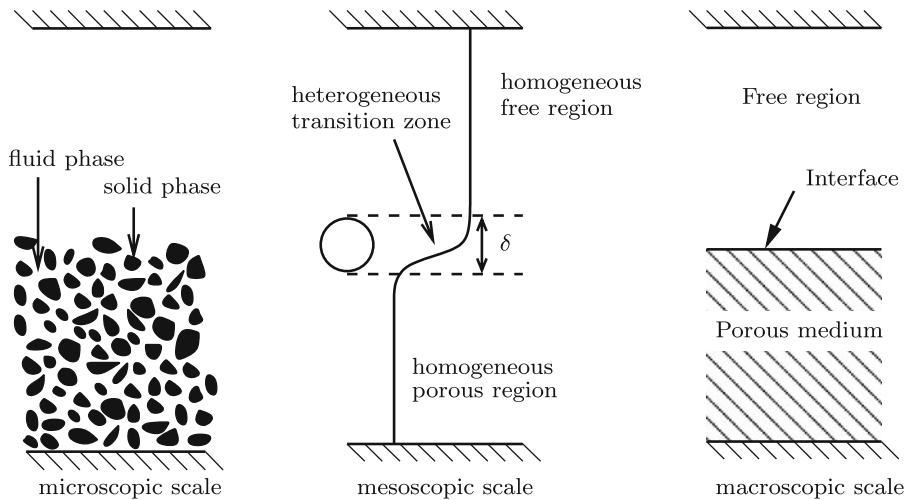


**Fig. 1** The interface between a homogeneous porous medium and a free fluid region at different scales of description

encounter strong but nevertheless continuous variations. The porosity, which is the average of the fluid indicator function, is represented in Fig. 1. The homogeneous porous region has a constant porosity  $\phi_p$ , the interfacial transition region is characterized by a spatially varying porosity and the homogeneous free fluid region has a porosity equal to unity. The thickness  $\delta$  of the transition region is of the order of magnitude of  $r_0$ .

After applying the same averaging volume in the whole domain, closure relations must be determined to obtain the effective properties of the medium. In the homogeneous porous region the validity of the closure relations can be proved under certain length scale constraints. In the interfacial transition region, these length scale constraints are not verified. To close the model in this region, two different approaches can be proposed. The first approach consists in deriving and solving a closure problem (Valdès-Parada et al. 2006, 2007b). However, the derivation of the closure problem is complex and its resolution is not always possible or is the subject of ongoing research. In the second approach, the form of the closed equation is postulated a priori and its validity is checked a posteriori. The effective properties in the interfacial transition region are deduced from the filtering of microscopic numerical simulations (Breugem et al. 2004; Chandesris and Jamet 2007). In this study, we will follow this second approach to determine the effective properties in the interfacial transition region. The transfers that occur in the interfacial transition region are modeled in this continuous model through these effective varying properties.

This first up-scaling step goes from a microscopic level where the characteristic length is the size of the solid inclusions to another level, which we named *mesoscopic scale*, where the fluid and solid phases have been replaced by an effective medium whose characteristic length is the scale of variation of the averaged quantities  $L$ . This first up-scaling is associated to the modeling of the porous medium. However, since the same averaging volume is applied in the whole domain and in particular in the vicinity of the interface, this up-scaling step introduces a new characteristic length, namely, the thickness  $\delta$  of the interfacial transition region.

## 2.2 Second Up-scaling Step

At the mesoscopic level, the physical fields vary continuously throughout the entire domain, albeit some of them (porosity, effective transport properties) vary very steeply within the interfacial transition region of thickness  $\delta$ . The macroscopic level corresponds to a description where the interface is discontinuous and where the effective transport properties are constant on both sides of the interface. Although the mesoscopic continuum description accounts for the underlying physic of the problem, the macroscopic level is generally more useful for the study of practical applications. Thus, a second up-scaling step is performed to go from the diffuse description of the interface to a discontinuous one. *This second up-scaling is associated to the modeling of the interface.* It has been thoroughly studied for liquid/liquid, liquid/vapor or liquid/solid interfaces (Emmerich 2003; Anderson et al. 1999; Edwards et al. 1991; Whitaker 1992).

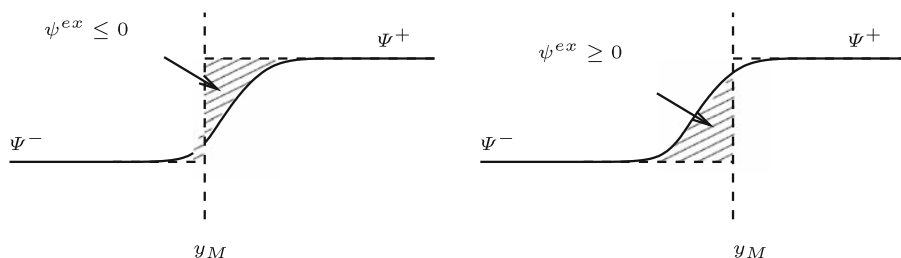
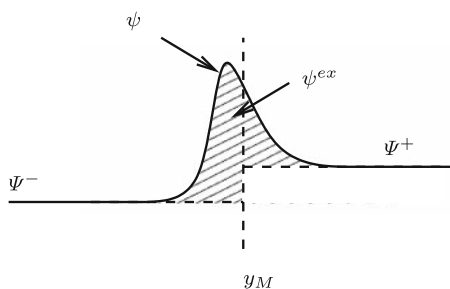
In this up-scaling, the continuous transition region, characterized by varying effective transport properties, is replaced by a discontinuous interface with constant effective transport properties on both sides of the interface. By doing this, one loses the local information of the mesoscopic model about the local transfers that occur in the interfacial transition region. However, the idea is to keep the macroscopic effects of the local transfers that occur within the interfacial transition region. For that, these macroscopic effects are modeled through jump boundary conditions that are assigned at the discontinuous interface. If the overall transfers are conserved during this up-scaling process, the mesoscopic and macroscopic solutions will not differ outside the interfacial transition region. Nevertheless, one expects that the two solutions will be different in the interfacial transition region since the local information of the mesoscopic model is lost.

To ensure the conservation of the overall transfers in the interfacial transition region, the idea (Edwards et al. 1991) is to compare the integrals of the meso- and macroscopic conservation equations in the entire domain. The difference represents the macroscopic effects of what has been lost by considering a macroscopic model instead of a mesoscopic one inside the transition region. As we will see in an example in the next section, this difference makes jumps appear at the interface and these jumps are related to excess-quantities. We recall that for any physical field  $\psi$ , its excess quantity is defined by:

$$\psi^{ex} = \int_{-\infty}^{y_M} (\psi(y) - \Psi^-) dy + \int_{y_M}^{+\infty} (\psi(y) - \Psi^+) dy \quad (2)$$

where  $\psi$  is the mesoscopic representation of the studied field,  $\Psi^+$  and  $\Psi^-$  are the macroscopic representations of this field in the two homogeneous regions, and  $y_M$  is the location of the discontinuous interface. In Fig. 2, the excess quantity is represented by the shaded area. It represents exactly the amount of the  $\psi$  field that is not taken into account by the macroscopic model in the interfacial transition region compared to the mesoscopic model.

It can be noticed that an excess quantity can be either positive or negative. It depends on how the transfer (or physical property) behaves in the interfacial transition region compared to how it behaves in the homogeneous regions. For example, for a reactive process, one can imagine that it can be inhibited in the interfacial transition region compared to the homogeneous regions. In this case, one would obtain a negative excess of reaction rate. To take into account the overall reaction rate in the interfacial transition region at the macroscopic scale, one will assign a negative excess reaction rate to the interface. On the contrary, if there

**Fig. 2** Illustration of a surface-excess quantity**Fig. 3** Sign of a surface-excess quantity depending on the location of the interface

is a catalyst in the interfacial transition region, one would obtain a positive excess reaction rate.

However, a positive or negative excess-quantity is not always related to a particular phenomenon that takes place in the interfacial transition region and not in the homogeneous regions. It is also related to a quantity that varies monotonically in the interfacial transition region, but has two different asymptotic values  $\Psi^-$  and  $\Psi^+$ . In this case, if the interface is located on one side of the transition region, one will obtain an excess quantity with a given sign. And if the interface is located on the other side of the transition region, the excess quantity will be of the opposite sign (see Fig. 3).

To illustrate the different steps of this multi-scale approach, we study in the next section a heat conduction problem in a fluid/porous domain.

### 3 Heat Conduction in a Fluid/Porous Domain

In this section, we consider a steady-state heat conduction problem in a domain partially filled with a porous medium, as the one presented in Fig. 1. We assume that a constant volumetric heat source,  $S_s$ , exists in the solid, whereas there is no heat source in the fluid. This heat source is introduced to show the consequences on the jump condition of a volumetric source term. The results obtained with and without this source term are discussed in Sect. 3.2.1. Noting  $k_f$  and  $k_s$  the microscopic thermal conductivities of the fluid and solid, respectively, the equations governing the system at the microscopic scale are given by:

$$\nabla \cdot (k_f \nabla T_f) = 0 \quad \text{in the fluid phase} \quad (3)$$

$$\nabla \cdot (k_s \nabla T_s) + S_s = 0 \quad \text{in the solid phase} \quad (4)$$

At the fluid–solid interface  $A_i$ , the boundary conditions are:

$$T_f = T_s \quad \text{on } A_i \quad (5)$$

$$\mathbf{n}_{fs} \cdot k_f \nabla T_f = \mathbf{n}_{fs} \cdot k_s \nabla T_s \quad \text{on } A_i \quad (6)$$

where  $\mathbf{n}_{fs}$  is the unit normal vector oriented outward from the fluid into the solid phase.

### 3.1 First Up-scaling Step

#### 3.1.1 Mesoscopic Governing Equations

The mesoscopic governing equations for  $\langle T_f \rangle^f$  and  $\langle T_s \rangle^s$  are obtained by applying the *phase average operator* (Whitaker 1999) to the microscopic Eqs. 3 and 4. Assuming the local thermal equilibrium, we have the approximation  $\langle T_f \rangle^f = \langle T_s \rangle^s = \langle T \rangle$ , where  $\langle T \rangle$  is the volume-averaged temperature defined by:

$$\langle T \rangle = \frac{1}{V} \int_V T dV = \phi \langle T_f \rangle^f + (1 - \phi) \langle T_s \rangle^s \quad (7)$$

A one-equation model is obtained by adding the mesoscopic equations obtained for  $\langle T_f \rangle^f$  and  $\langle T_s \rangle^s$  (Kaviany 1995, Chap. 3):

$$\begin{aligned} \nabla \cdot [(\phi k_f + (1 - \phi) k_s) \nabla \langle T \rangle] + \nabla \cdot \left[ \frac{k_f - k_s}{V} \int_{A_i} \mathbf{n}_{fs} \check{T}_f dA \right] \\ + (1 - \phi) S_s = 0 \end{aligned} \quad (8)$$

where  $\check{\psi}_f = \psi_f - \langle \psi_f \rangle^f$ . The assumption  $r_0 \ll L$  is used to derive this equation. To close this equation, one still needs to model the term of the left-hand side of Eq. 8 that involves microscopic quantities through  $\check{T}_f$ .

For the homogeneous porous region, it has been shown (Nozad et al. 1985) that Eq. 8 reduces to:

$$\nabla \cdot [\mathbf{k}_p^{\text{eff}} \cdot \nabla \langle T \rangle] + (1 - \phi_p) S_s = 0 \quad (9)$$

where  $\mathbf{k}_p^{\text{eff}}$  is the effective thermal conductivity tensor of the porous medium.

In the homogeneous free fluid region, the porosity is equal to one. Assuming that  $r_0 \ll L$ , we have the approximation  $\langle T \rangle = \langle T_f \rangle^f \approx T_f$ . Finally, since there is no solid, Eq. 8 reduces to the heat conduction equation valid at the microscopic scale in the fluid phase Eq. 4.

In the interfacial transition region, the resolution of the closure problem is much more complex. First, the length scale constraint  $r_0 \ll L$  and the local thermal equilibrium assumption used to derive Eq. 8 are not valid and a more complex equation is obtained as the result of the averaging process (see Valdès-Parada et al. (2007a) for example). Then, the determination and the resolution of the closure problem associated to the obtained equation are very complex. First, the length scale constraint  $r_0 \ll L$  used to simplify the closure problem in the homogeneous porous region is not valid. Second, the property of periodicity of the unit cell used to solve the closure problem in the homogeneous porous region disappears. Thus, as mentioned in Sect. 2.1, we follow another approach. We postulate the form of the closed equation and deduce the associated effective properties by filtering microscopic numerical simulations.

To postulate the form of the closed equation in the interfacial transition region, we suppose that no other phenomenon than the one acting in the homogeneous regions have to

be taken into account. Thus, we assume that there exists an effective thermal conductivity tensor  $\mathbf{k}^{\text{eff}}(\mathbf{x})$  such that the interfacial transition region is well represented by the following equation:

$$\nabla \cdot [\mathbf{k}^{\text{eff}}(\mathbf{x}) \cdot \nabla \langle T \rangle] + (1 - \phi(\mathbf{x})) S_s = 0 \quad (10)$$

where  $\mathbf{x}$  is the coordinate vector  $\mathbf{x} = (x, y, z)$ . A profile of  $\mathbf{k}^{\text{eff}}(\mathbf{x})$  for one particular geometry will be deduce by filtering a microscopic numerical simulation in the next section. Finally, at the mesoscopic scale, the problem is governed by a single transport equation (10).

### 3.1.2 Effective Thermal Conductivity in the Interfacial Region

The objective of this section is to show how to determine the effective thermal conductivity at the mesoscopic scale  $k^{\text{eff}}(y)$  for a two-dimensional porous medium made of cubes as shown in Fig. 4a. Because the problem is periodic in the  $x$ -direction, it is sufficient to simulate only a single column of cubes and to apply periodic boundary conditions in the horizontal direction. For practical reasons regarding the implementation of the volume-averaging filter, we have computed three columns of cubes. In the  $y$ -direction five cubes have been used. The idea is to take enough cubes to ensure that in the core of the porous medium the averaged properties are uniform, but not too many to reduce the computational cost. The distance between two cubes is  $d_p$  and the size of a cube is  $2d_p$ . Thus,  $\phi_p = 5/9$ . The origin of the  $y$ -axis has been arbitrarily located one  $d_p$  above the last cube and the ratio  $d_p/H$  was fixed at  $1/16 = 0.0625$ . The ratio  $k_s/k_f$  has been fixed at 50 to be consistent with [Sahraoui and Kaviany \(1992\)](#). A constant and uniform temperature  $T^{\text{imp}}$  is imposed at the lower wall, such that  $T = 10$  at the upper wall. This value is arbitrary, since in this problem, the temperature is defined up to a constant. A constant and uniform heat flux  $q^{\text{imp}} = -1$  is imposed at the upper wall of the domain. For the constant volumetric heat source in the solid  $S_s$ , we arbitrary choose a Damkohler number of 10, where  $D_{\text{am}} = S_s H / |q^{\text{imp}}|$ . In this case, the Damkohler number compares the heat flux coming from a heat source to the heat flux evacuated by conduction.

The microscopic temperature field is obtained by solving numerically the system 3–4 on a uniform Cartesian mesh. For the spatial discretization, the finite-volume method is used with a second-order central-differencing scheme. The obtained microscopic fluid temperature field is presented in Fig. 4b.

The mesoscopic fields  $\langle T \rangle(y)$  and  $\phi(y) = \langle \chi \rangle$ , where  $\chi$  is the fluid phase indicator function, are obtained by volume-averaging their corresponding microscopic fields. This averaging is performed using the averaging volume and the cellular weighting function  $m(\mathbf{x})$  proposed by [Quintard and Whitaker \(1994\)](#), which are adapted to ordered porous medium:

$$m(\mathbf{x}) = \begin{cases} \Pi_{i=1}^2 (l - |x_i|) / l^2, & |x_i| \leq l \\ 0, & |x_i| > l \end{cases} \quad (11)$$

where  $l$  is the length of the unit cell ( $l = 3d_p$  in this example) and  $x_i$  is the coordinate in direction  $i$ . The averaging volume corresponding to our geometry is presented in Fig. 4a. It can be noticed that since the filtering process is defined as a convolution product, it ensures the continuity of the physical variables at the mesoscopic scale. Furthermore, since the cellular weighting function  $m(\mathbf{x})$  is continuous and piece-wise differentiable, it ensures that the gradient of the mesoscopic variables is continuous. The obtained porosity profile is presented Fig. 5c. It is constant, equal to  $\phi_p$ , for  $y \leq -3d_p$ , varying in the interfacial transition region for  $-3d_p \leq y \leq 2d_p$  and constant equals to unity for  $y \geq 2d_p$ . The mesoscopic temperature profile is presented Fig. 5a along with the microscopic temperature profile at  $x/H = 0$ .

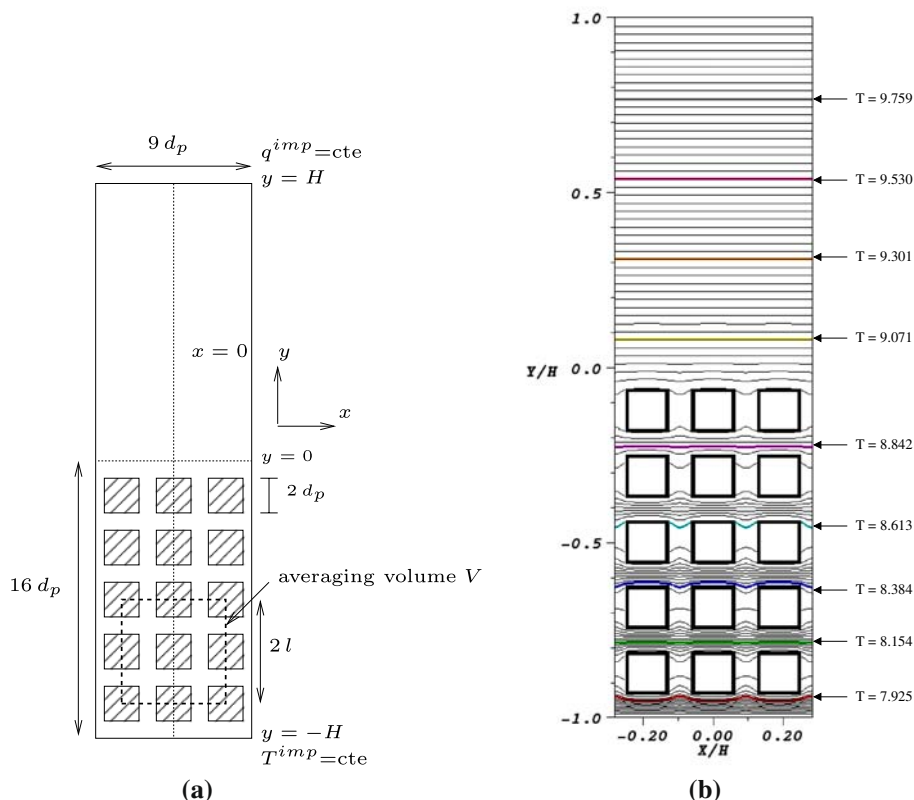


**Fig. 4** Heat conduction in a fluid/porous domain. **a** Description of the geometry. **b** Iso-contours of the microscopic fluid temperature  $T_f(x, y)$

We introduce the mesoscopic heat flux,  $q(y)$ , defined by:

$$q(y) = -k^{\text{eff}}(y) \frac{d\langle T \rangle}{dy} \quad (12)$$

It is such that:

$$\frac{dq}{dy} = (1 - \phi(y)) S_s \quad (13)$$

Since the heat flux at the upper boundary is known,  $q(H) = q^{\text{imp}}$ ,  $q(y)$  can be determined unambiguously from the porosity profile  $\phi(y)$ . Then, the effective thermal conductivity can be deduced using Eq. 12. The corresponding profiles are presented Fig. 5b and c. The effective thermal conductivity is constant in both homogeneous regions (for  $y \leq -3d_p$  and  $y \geq 2d_p$ ) and varies smoothly across the interfacial transition region. Thus, the effective properties of the porous medium ( $\phi$  and  $k^{\text{eff}}$ ) are uniform in the core of the porous medium ( $y \leq -3d_p$ ) which confirms our choice of taking only five cubes in the  $y$  direction.



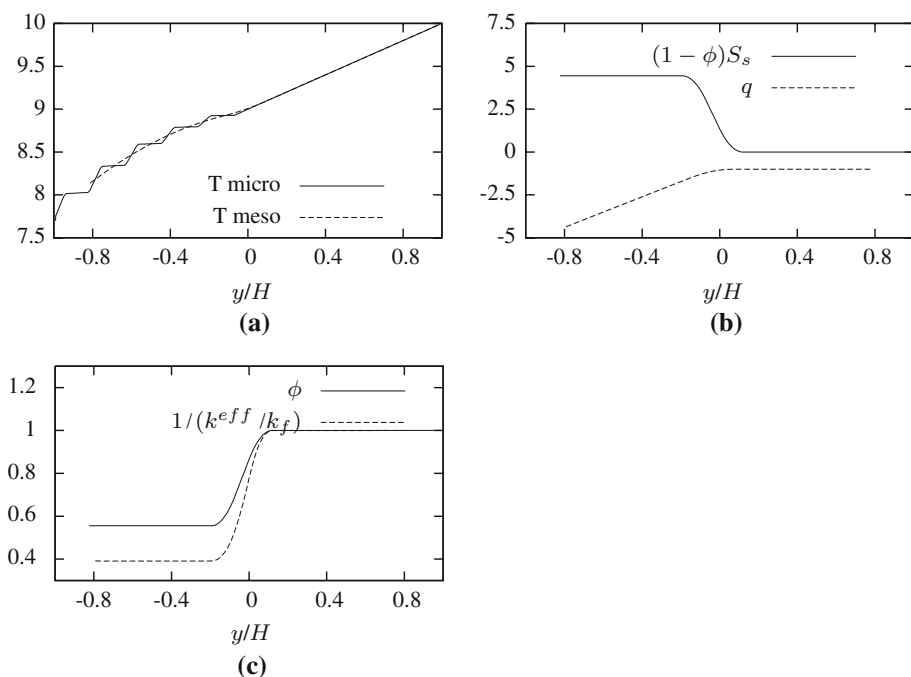


**Fig. 5** Results at the mesoscopic scale. **a** Microscopic and mesoscopic temperatures. **b** Heat source and heat flux at the mesoscopic scale. **c** Porosity and effective thermal conductivity

### 3.2 Second Up-scaling Step

The variations of  $\phi(y)$  and  $k^{eff}(y)$  in the interfacial transition region obtained in the last section account for the local heat conduction transfer that occurs in this region. However, for practical applications, one will distinguish only their constant asymptotic values. The objective of this section is to derive the jump conditions that must be applied at the interface at the macroscopic scale, to still account for the overall heat transfer. To avoid any confusion, the temperature solution of the macroscopic problem is noted  $\tilde{T}_f$  in the free fluid region and  $\tilde{T}_p$  in the porous region.

#### 3.2.1 Heat Flux Jump Condition

In order to ensure the overall conservation of energy, the jump conditions are obtained by integrating in the entire domain, the difference between the mesoscopic and the macroscopic equations (see Sect. 2.2). In the free fluid region (i.e., for  $y_M < y < H$ ), this difference is given by:

$$\frac{d}{dy} \left[ k^{eff}(y) \frac{d\langle T \rangle}{dy} - k_f \frac{d\tilde{T}_f}{dy} \right] + (1 - \phi(y)) S_s = 0 \quad (14)$$

In the porous region (i.e., for  $-H < y < y_M$ ), it is given by:

$$\frac{d}{dy} \left[ k^{eff}(y) \frac{d\langle T \rangle}{dy} - k_p^{eff} \frac{d\tilde{T}_p}{dy} \right] + (\phi_p - \phi(y)) S_s = 0 \quad (15)$$

Integrating Eq. 14 between  $y_M$  and  $H$  and Eq. 15 between  $-H$  and  $y_M$ , and then adding the resulting equations, one gets:

$$\begin{aligned} & k_f \frac{d\tilde{T}_f}{dy} \Big|_{y_M^+} - k_p^{\text{eff}} \frac{d\tilde{T}_p}{dy} \Big|_{y_M^-} + \left[ k^{\text{eff}}(y) \frac{d\langle T \rangle}{dy} - k_f \frac{d\tilde{T}_f}{dy} \right] \Big|_H \\ & - \left[ k^{\text{eff}}(y) \frac{d\langle T \rangle}{dy} - k_p^{\text{eff}} \frac{d\tilde{T}_p}{dy} \right] \Big|_{-H} + (1 - \phi)^{ex} S_s = 0 \end{aligned} \quad (16)$$

where the excess quantity is defined using Eq. 2. The two terms in brackets vanish. Indeed, by construction, the macroscopic model is sought for such that it is equal to the mesoscopic solution within each homogeneous regions and in particular at the boundaries of these regions, i.e., at  $-H$  and  $H$ . This yields:

$$- k_f \frac{d\tilde{T}_f}{dy} \Big|_{y_M^+} + k_p^{\text{eff}} \frac{d\tilde{T}_p}{dy} \Big|_{y_M^-} = (1 - \phi)^{ex} S_s \quad (17)$$

The difference between the heat fluxes at the interface is equal to a source of heat,  $(1 - \phi)^{ex} S_s$ , concentrated at the interface. Since the porosity varies smoothly in the transition region and because the two asymptotic values of the heat source are different (0 in the free fluid region and  $(1 - \phi_p) S_s$  in the homogeneous porous region), the value of this excess quantity will depend on the location of the interface (see Fig. 3). This excess heat source appears not because there is a particular phenomenon at the interface, but because the heat source is not correctly modeled by the macroscopic model. Indeed, in the macroscopic model, only the two asymptotic values of the heat source are represented, whereas in the mesoscopic model, all the local variations (within the interfacial region) of the heat source are accounted for. When there is no heat source,  $S_s = 0$ , nothing is forgotten by the macroscopic model compared to the mesoscopic one and a continuous conductive heat flux is obtained as in Jamet and Chandesris (2008). The heat flux jump condition (17) is such that the overall source of heat of the mesoscopic model is taken into account in the macroscopic model.

### 3.2.2 Temperature Jump Condition

To determine the second boundary condition, we use the mesoscopic heat flux  $q(y)$  that satisfies Eq. 13 and is therefore known at the mesoscopic scale (see Sect. 3.1.2). The mesoscopic conduction equation can be rewritten in the following way:

$$\frac{d\langle T \rangle}{dy} = - \frac{q(y)}{k^{\text{eff}}(y)} \quad (18)$$

Following the same reasoning as in the previous section, one gets:

$$\tilde{T}_f \Big|_{y_M^+} - \tilde{T}_p \Big|_{y_M^-} = - \left( \frac{q}{k^{\text{eff}}} \right)^{ex} \quad (19)$$

This temperature jump condition involves the excess quantity of the flux  $q$  times the thermal resistance  $1/k^{\text{eff}}$ . These two quantities are not represented in the same way in the interfacial transition region at the meso- and macroscopic scales. The excess quantity represents the overall difference. Assigned to the interface via the temperature jump condition, it ensures that the overall transfer (flux time thermal resistance) is conserved in the up-scaling process.

Equations 17 and 19 show that for a heat conduction problem in a fluid/porous domain, the origin of the heat flux jump at the interface is related to the excess of the heat source at

the interface and the origin of the temperature jump is related to the excess of the flux time the thermal resistance.

### 3.2.3 Excess Quantities and Location of the Interface

The jump conditions (17) and (19) involve excess quantities. Given the definition (2) of an excess quantity, it can be shown that its value depends on the position of  $y_M$  when  $\Psi^- \neq \Psi^+$ . To show this, a particular position  $y_\psi$  is introduced for which the sum of the two integral terms of equation (2) is zero:

$$\int_{-\infty}^{y_\psi} (\psi(y) - \Psi^-) dy + \int_{y_\psi}^{+\infty} (\psi(y) - \Psi^+) dy = 0 \quad (20)$$

This particular position  $y_\psi$  is named the center of gravity of the profile of  $\psi$ . Using this definition, one gets, when  $\Psi^-$  and  $\Psi^+$  are constants:

$$\psi^{ex} = (y_\psi - y_M)(\Psi^- - \Psi^+) \quad (21)$$

which shows that, when  $\Psi^-$  and  $\Psi^+$  are constants, the excess quantity depends linearly on  $y_M$ . Thus, when  $\Psi^- \neq \Psi^+$ , which is the case in our problem, the value of the excess quantities does depend on the location of the interface inside the transition region. Nevertheless, this dependence of the excess quantity and thus of the jump coefficient, on the location of the interface, compensates the fact that the macroscopic problems are different in the two homogeneous regions ( $\Psi^- \neq \Psi^+$ ). Thus, changing the interface location modifies the zone of influence of a given macroscopic model. Finally, the value of the excess quantity is such that, whatever the location of the discontinuous interface inside the transition region, the overall amount of a given quantity is conserved at the macroscopic scale via the two asymptotic values of this quantity in the homogeneous regions and via the excess quantity assigned at the interface.

To illustrate this point, we compute the macroscopic solutions obtained using the boundary conditions (17) and (19) for three different values of  $y_M$ . First, we determine the value of the two excess quantities, for different locations of the interface using the profiles of  $\phi$ ,  $q$ , and  $k^{\text{eff}}$  determined in Sect. 3.1.2. For the heat source  $(1 - \phi)^{ex} S_s$ , since its asymptotic values are constant, its value depends linearly on  $y_M$ . For the other excess quantity, its dependence on  $y_M$  is quadratic because the asymptotes of  $q$  in the homogeneous regions are not constant, but linear in  $y$ . The values of the excess quantities are presented in Table 1. In Fig. 6, the macroscopic temperatures obtained for different positions of the interface are presented along with the mesoscopic temperature profile. This figure shows that the macroscopic problem is indeed equivalent to the mesoscopic one, whatever the position of the interface in the interfacial region. Furthermore, the mesoscopic and the macroscopic solutions differ only, as expected, in the transition region (Fig. 6b).

**Table 1** Value of the excess quantities for different positions of the interface

$y_M/H$	$(1 - \phi)^{ex} S_s$	$(q/k^{\text{eff}})^{ex}$
0.1	-0.583	-0.0994
0	-0.139	-0.0279
-0.1	0.306	0.0337

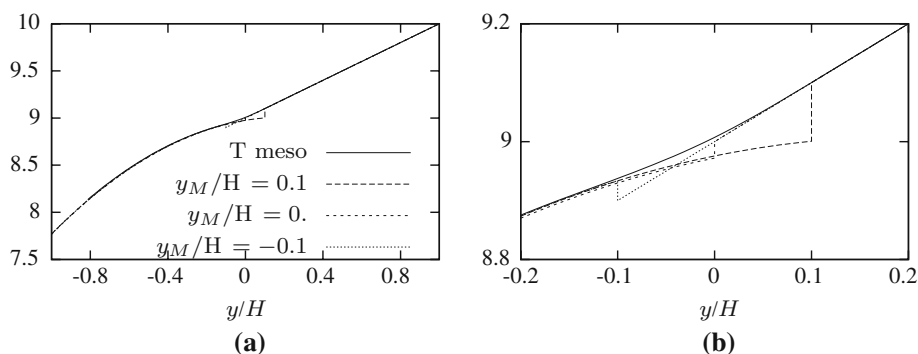


**Fig. 6** **a** Comparison of the mesoscopic and macroscopic solutions for different positions of the interface. **b** Zoom on the interfacial region

#### 4 Laminar Flow over a Porous Medium

In this section, we consider the case of a Poiseuille flow over a porous medium. The objective is not to detail the steps of our two-step up-scaling analysis which has been carried out in Chandesris and Jamet (2006, 2007). However, we aim at illustrating why this problem is more complex than the heat conduction problem and requires the use of another method for the second up-scaling step. Furthermore, our objective is to show how the results of this multi-scale analysis can be used to study the empirical slip boundary condition of Beavers and Joseph.

##### 4.1 First Up-scaling Step

For a Poiseuille flow over a porous medium, the problem is governed at the microscopic scale by the Stokes equations on the fluid phase:

$$\nabla \cdot \mathbf{u} = 0 \quad (22)$$

$$\mu \nabla^2 \mathbf{u} = \nabla p \quad (23)$$

$$\mathbf{u} = 0 \quad \text{on } A_i \quad (24)$$

The mesoscopic governing equations are obtained by applying the *phase average operator* to the Eqs. 22 and 23 (Whitaker 1999, Chap. 4). After this averaging procedure, closure relations must be determined to model the terms that involve microscopic quantities.

In the homogeneous porous region, the volume-averaged momentum equation reduces to the Darcy–Brinkman equation:

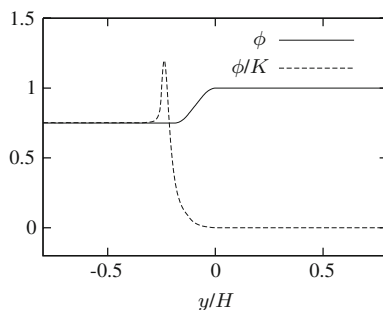
$$\frac{\mu}{\phi_p} \nabla^2 \langle \mathbf{u} \rangle = \nabla \langle p \rangle^f + \mu \mathbf{K}_p^{-1} \cdot \langle \mathbf{u} \rangle \quad (25)$$

where  $\mathbf{K}_p$  is the permeability tensor in the homogeneous porous region.

In the homogeneous free fluid region, assuming that  $r_0 \ll L$ , we have the approximations  $\langle \mathbf{u} \rangle \approx \mathbf{u}$  and  $\langle p \rangle^f \approx p$ . Furthermore, since there is no solid and since the porosity is equal to 1, the volume-averaged momentum equation reduces to the Stokes equation (23).

In the interfacial transition region the problem is much more complex. As explained in Sect. 2.1, we postulate the form of the closed equation and deduce the associated effective properties by filtering microscopic numerical simulations. Thus, we assume that there exists

**Fig. 7** Non-dimensional porosity and permeability profiles obtained by filtering microscopic simulations



a permeability tensor  $\mathbf{K}(\mathbf{x})$  such that the interfacial transition region is well represented by the following equation:

$$\frac{\mu}{\phi(\mathbf{x})} \nabla^2 \langle \mathbf{u} \rangle = \nabla \langle p \rangle^f + \mu \mathbf{K}(\mathbf{x})^{-1} \cdot \langle \mathbf{u} \rangle \quad (26)$$

Here, we have assumed that the effective viscosity is well represented by using  $\mu_{\text{eff}} = \mu/\phi$ . The permeability tensor can be deduced from microscopic simulations using the same filtering process and filter as those presented in Sect. 3.1.2 (see Breugem et al. (2004) for a detailed example). In the subsequent section, the porosity and permeability profiles obtained for a porous medium made of cubes, where the size and the distance between two cubes is equal, will be used (see Chandesris and Jamet (2007) for a detailed description of the geometry). These profiles are presented in Fig. 7. The porosity and the inverse of the permeability are constant in the two homogeneous regions and vary smoothly across the interfacial transition region.

## 4.2 Second Up-scaling Step

The objective of this section is to show how to derive the jump conditions that must be applied at the macroscopic scale for the case of a Poiseuille flow over a porous medium, i.e., when the problem is one-dimensional.

### 4.2.1 Surface-Excess Theory

As shown in Sect. 3.2.1 the jump conditions are obtained by integrating in the entire domain, the difference between the mesoscopic and the macroscopic governing equations. Following the same reasoning, one gets:

$$\mu \left. \frac{d\tilde{u}_f}{dy} \right|_{y_M^+} - \mu \left. \frac{d\tilde{u}_p}{dy} \right|_{y_M^-} = \phi^{ex} \frac{dp}{dx} + \mu \left( \frac{\phi}{K} \langle u \rangle \right)^{ex} \quad (27)$$

where  $\tilde{u}_f$ , and,  $\tilde{u}_p$ , are the volume-averaged velocity solution of the macroscopic problem in the free fluid region, and in the homogeneous porous region. Thus, this method shows that the stress jump condition depends on two excess quantities: the pressure surface-excess force  $\phi^{ex} dp/dx$  and the friction surface-excess force  $\mu(\phi/K \langle u \rangle)^{ex}$ . These surface-excess forces represent the amount of the force that is not correctly modeled by the macroscopic model compared to the mesoscopic one in the interfacial transition region.

However, the stress jump condition (27) is not closed. Indeed, the friction surface-excess force  $\mu(\phi/K \langle u \rangle)^{ex}$  depends on an unknown mesoscopic variable  $\langle u \rangle$ . Thus, contrary to

the heat conduction problem, for the Poiseuille flow problem, the surface-excess theory is not sufficient to derive a closed jump condition. To overcome this difficulty, we have used in [Chandesris and Jamet \(2006\)](#) another method, the matched asymptotic expansion method, which also allows to perform this second up-scaling step. This method, which is more technical, allows to derive a closed form for the friction surface-excess force, i.e., the friction surface-excess force is expressed using only macroscopic variables.

#### 4.2.2 Matched Asymptotic Expansion Method

The idea of this method is to solve analytically, using an asymptotic expansion in  $\varepsilon$ , the equations governing the problem at the mesoscopic scale. This asymptotic expansion is feasible because a small parameter,  $\varepsilon = \delta/H$ , is present in the mesoscopic equation (26) through the porosity and permeability profiles. As  $\varepsilon$  tends to zero, the transition region tends to a discontinuous surface. Thus, the result obtained using the asymptotic expansion is both an approximated solution at a given order of the mesoscopic problem and the solution of a macroscopic problem with a discontinuous interface for which the boundary conditions can be made explicit. Thus, this method allows to derive analytically, and at a given order, the boundary conditions of the macroscopic problem such that the macroscopic problem is indeed equivalent to the mesoscopic one.

The technical steps of the method are presented in [Chandesris and Jamet \(2006\)](#). At order 0 in  $\varepsilon$ , the velocity  $\langle u \rangle_{(0)}$  and the stress are continuous at the interface. At order 1 in  $\varepsilon$ , one gets:

$$\tilde{u}_f|_{y_M^+} - \tilde{u}_p|_{y_M^-} = 0 \quad (28)$$

$$\mu \frac{d\tilde{u}_f}{dy} \Big|_{y_M^+} - \mu \frac{d\tilde{u}_p}{dy} \Big|_{y_M^-} = \phi^{ex} \frac{dp}{dx} + \mu \left( \frac{\phi}{K} \right)^{ex\Delta} \langle u \rangle_{(0)} \Big|_{y_M} \quad (29)$$

where  $\tilde{u} = \langle u \rangle_{(0)} + \varepsilon \langle u \rangle_{(1)}$  is the macroscopic velocity, solution of the mesoscopic problem at order 1 and

$$\left( \frac{\phi}{K} \right)^{ex\Delta} = (y_{f_f} - y_M) \left( \frac{\phi_p}{K_p} \right) \quad (30)$$

where  $y_{f_f}$  is the center of gravity of the friction force. The determination of  $y_{f_f}$  is not direct and requires to perform one numerical simulation at the mesoscopic scale ([Chandesris and Jamet 2007](#)). However, we have shown that its value is independent of  $H$  and thus, this quantity is indeed representative of the momentum transfer in the interfacial transition region. Finally, comparing Eqs. 27 and 29, one can see that the method of matched asymptotic expansion allows to obtain a closed form for the friction surface-excess force.

For the porosity and permeability profiles presented in Fig. 7,  $y_{f_f}/H = -0.094$  and  $y_{f_f}/H = -0.11$ . The macroscopic velocity obtained for different positions of the interface is presented along with the mesoscopic velocity profile in Fig. 8a. The corresponding values of the two excess quantities are presented in Table 2. Figure 8a shows that the macroscopic solutions obtained using the stress jump condition (29) agree very well with the mesoscopic solution in the two homogeneous regions, whatever the position of the interface in the transition region (provided that the variation of the jump parameters with the interface position, which are known analytically, is accounted for).

Thus, different methods can be used to perform this second up-scaling step. The surface-excess theory is easy to carry on. However, the obtained boundary conditions, which are

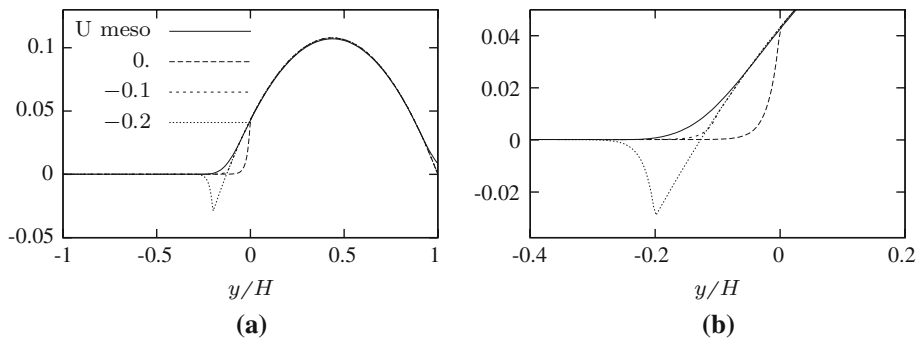


**Fig. 8** **a** Comparison of the mesoscopic and macroscopic solutions for different positions of the interface  $y_M/H = 0; -0.1; -0.2$ . **b** Zoom on the interfacial region

**Table 2** Value of the excess quantities for different positions of the interface

$y_M/H$	$\phi^{ex}$	$K_p (\phi/K)^{ex\Delta}$
0	$2.34 \times 10^{-2}$	$-8.25 \times 10^{-2}$
-0.1	$-0.156 \times 10^{-2}$	$-0.75 \times 10^{-2}$
-0.2	$-2.66 \times 10^{-2}$	$6.75 \times 10^{-2}$

expressed through excess quantities, are not always closed. The method of matched asymptotic expansion is more technical, but allows to obtain closed expressions for the boundary conditions.

#### 4.3 Beavers and Joseph's Slip Boundary Condition

In the previous section, we have shown that the boundary conditions (28) and (29) account for the momentum transfer at the fluid/porous interface when the Darcy–Brinkman model, with constant porosity and permeability, is used in the homogeneous porous region. The objective of this section is to go further, to use the Darcy model in the porous region and determine the conditions under which the well-known semi-empirical Beavers and Joseph's slip boundary condition can be applied.

To derive this boundary condition, we start from the results obtained in the previous section. Because of the exponential decay of the velocity in the porous domain, it is possible to relate  $d\tilde{u}_p/dy|_{y_M^-}$  to the velocity at the interface  $u_B = \tilde{u}_p(y_M)$ . Thus, the jump condition (29) becomes:

$$\left. \frac{d\tilde{u}_f}{dy} \right|_{y_M^+} = \sqrt{\frac{\phi_p}{K_p}} (u_B - U_D) + \frac{\phi^{ex}}{\mu} \frac{dp}{dx} + \left( \frac{\phi}{K} \right)^{ex\Delta} \langle u \rangle_{(0)} \Big|_{y_M} \quad (31)$$

The same macroscopic solutions are obtained in the homogeneous regions, i.e., outside the interfacial region, by solving (i) the Darcy–Brinkman model and the Stokes model connected with the boundary conditions (28) and (29) or (ii) the Darcy model and the Stokes model connected with the boundary condition (31). This result is illustrated in Fig. 9, where the mesoscopic velocity is presented along with the two macroscopic results.

The main drawback of the boundary condition (31) is that it depends on the macroscopic unknown  $\langle u \rangle_{(0)}$ . However, if the discontinuous interface is located in the transition region,

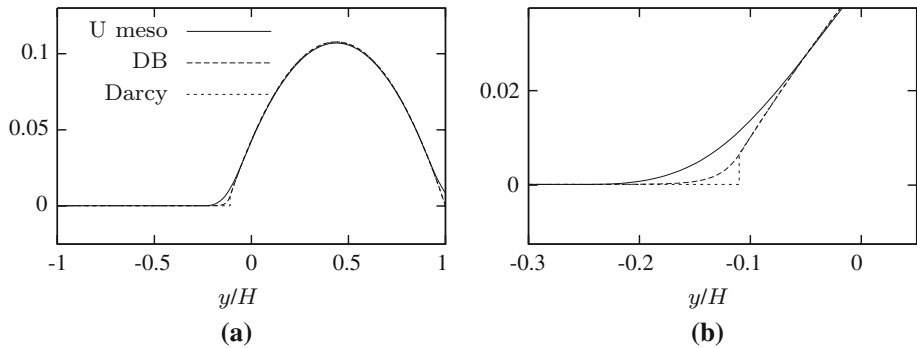


**Fig. 9** **a** Comparison of the Darcy and Darcy–Brinkman (DB) models ( $y_M = y_{fi}$ ). **b** Zoom on the interfacial region

such that the friction surface-excess force vanishes, i.e., for  $y_M = y_{fi}$  one has  $(\phi/K)^{ex\Delta} = 0$  and gets:

$$\left. \frac{d\tilde{u}_f}{dy} \right|_{y_M^+} = \sqrt{\frac{\phi_p}{K_p}} (u_B - U_D) + \frac{\phi^{ex}}{\mu} \frac{dp}{dx} \quad (32)$$

The above boundary condition is a generalization of the Beavers and Joseph's relation (1) in the sense that it involves a second term that depends on the pressure gradient. Since  $U_D = -(K_p/\mu)(dp/dx)$ , relation (32) can be rewritten in the following form:

$$\left. \frac{d\tilde{u}_f}{dy} \right|_{y_M^+} = \sqrt{\frac{\phi_p}{K_p}} \left[ u_B - U_D \left( 1 - \frac{\phi^{ex}}{\sqrt{\phi_p K_p}} \right) \right] \quad (33)$$

If  $\phi^{ex} = 0$ , the relation (1) is recovered with  $\alpha = \sqrt{\phi_p}$ . Thus, the above analysis shows that the Beavers and Joseph's semi-empirical relation (1) is exactly recovered when (i) the two surface-excess forces vanish exactly at the same location, i.e.,  $y_\phi = y_{fi}$  and (ii) the discontinuous interface is located such that  $y_M = y_\phi = y_{fi}$ .

The solution of the Stokes equation (23) with a no slip condition at the upper wall,  $u(H) = 0$ , and the boundary condition (33) at  $y = y_M$  is given by:

$$u(y) = \frac{-U_D}{2K_p} \left( (y - y_M)^2 + 2\sqrt{K_p} \left( \sqrt{\phi_p} + \phi^{ex}/\sqrt{K_p} \right) (y - y_M) \right) + u_B \left( 1 + \sqrt{\frac{\phi_p}{K_p}} y \right) \quad (34)$$

with

$$u_B = \frac{U_D}{2} \left( \frac{\sigma^2 + 2\sigma \left( \sqrt{\phi_p} + \phi^{ex}/\sqrt{K_p} \right)}{1 + \sigma\sqrt{\phi_p}} \right) \quad (35)$$

and  $\sigma = (H^+ - y_M)/\sqrt{K_p}$ . When  $\phi^{ex} = 0$ , we recover the Beavers and Joseph (1967) solution with  $\alpha = \sqrt{\phi_p}$ .

The parameter  $\sigma$  involves a macroscopic length  $(H^+ - y_M)$  and a length characteristic of the size of the solid inclusion  $\sqrt{K_p}$ . However, since the size of the filter  $r_0$  is also directly



related to both the size of the solid inclusion and is of the order of the size of the transition region, the length  $\sqrt{K_p}$  is of the order of the interfacial transition region. Thus, the parameter  $\sigma$  is characteristic of the ratio of the size of the free fluid region over the size of the transition region. The size of the free fluid region is generally larger than the size of the transition region. Typical values of  $\sigma$  are in the range [5–120] (Beavers and Joseph 1967). Equation 35 shows that for such values of  $\sigma$ , the slip velocity is much larger than the Darcy velocity ( $u_B/U_D \sim \sigma/\sqrt{\phi_p}$ ) and the latter can thus be neglected in the boundary conditions (1) and (33). Thus, if  $\phi^{ex}/\sqrt{\phi_p K_p}$  is smaller than or of order 1, which is usually the case, and if the values of  $\sigma$  are relatively large, the boundary conditions (33) and (1) reduce to the same relation:

$$\left. \frac{d\tilde{u}_f}{dy} \right|_{y_M^+} = \sqrt{\frac{\phi_p}{K_p}} u_B \quad (36)$$

and are therefore equivalent. Finally, for large values of  $\sigma$ , the only constraint to recover the Beavers and Joseph's semi-empirical relation (1) is to locate the discontinuous interface such that the friction surface-excess force vanishes, i.e., at  $y_M = y_{f_i}$ . Equation 36 also shows that the ratio  $u_B/\sqrt{K_p}\dot{\gamma}$  (where  $\dot{\gamma}$  is the shear rate  $d\tilde{u}_f/dy$ ) studied by James and Davis (2001), Tachie et al. (2004), and others is simply given by  $1/\sqrt{\phi_p}$ . But, as for the Beavers and Joseph's semi-empirical relation, this simple relation is valid only for the particular position of the interface  $y_M = y_{f_i}$ .

This analysis is illustrated on the particular porous geometry studied in the previous section. At the mesoscopic scale, we solve Eq. 26 with the permeability and porosity profiles presented in Fig. 7 ( $y_{f_i}/H = -0.11$  and  $y_\phi/H = -0.094$ ) for different heights  $H^+$  of the free fluid channel. At the macroscopic scale, the Darcy and the Stokes models are connected using relation (33) at  $y_M = y_{f_i}$ . The solution is given by Eq. 34. The macroscopic solution is presented along with the mesoscopic solution in Fig. 10a. The macroscopic solution obtained using the Beavers and Joseph's semi-empirical relation (1) with  $\alpha = \sqrt{\phi_p}$  and  $y_M = y_{f_i}$  is also presented for comparison. The velocity profile in the free fluid region is very well predicted by the Beavers and Joseph's relation (1). As expected and since  $\sigma$  is relatively large in this case ( $\sigma \sim [40\text{--}90]$ ), the results obtained using the boundary conditions (33) and (1) do not differ. These boundary conditions actually reduce to the boundary condition (36), which is sufficient to predict the velocity profile in the free fluid region.

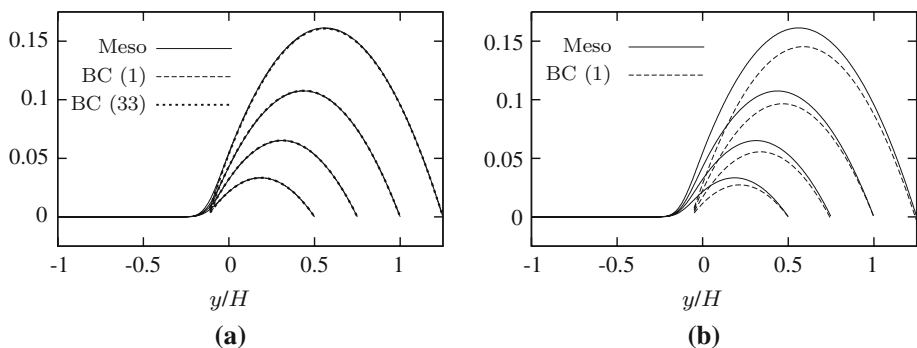


**Fig. 10** Mesoscopic and macroscopic results. **a** The interface is located in  $y_M = y_{f_i} = -0.11$ . **b** The interface is arbitrary located in  $y_M/H = -0.05$

In Fig. 10b, we present the results obtained using relation (1) with  $\alpha = \sqrt{\phi_p}$  when the interface is not located at  $y_M = y_{fi}$  but at another arbitrary location inside the interfacial transition region. The velocity profile is not correctly predicted. This result illustrates the sensitivity of the Beavers and Joseph's relation (1) to the precise location of the interface inside the transition region. For the same value of the parameter  $\alpha$ , the velocity in the free fluid region is very well predicted when  $y_M = y_{fi}$  (Fig. 10a) and not at all for another position of  $y_M$  (Fig. 10b). This shows that, the precise location of the interface inside the transition region is a crucial point to accurately predict the velocity profile in the free fluid region while using the Beavers and Joseph's semi-empirical boundary condition (1). A discussion on the value of  $\alpha$  loses some of its sense without a discussion on the location of the discontinuous interface as illustrated in Fig. 10.

Finally, it can be noticed that if one takes  $\alpha = \sqrt{\phi_p}$ , one cannot recover the experimental values proposed by Beavers and Joseph, which go up to 4. However, this analysis shows that a crucial point in the analysis is the knowledge of the exact location of the interface inside the transition region (Fig. 10). In the Beavers and Joseph's experiments, this difficulty is materialized through the choice of the location of the adjustable divider plate in the transition region which allows to measure the mass flow rate in the free fluid region. Since this location is not precisely known for the Beavers and Joseph's experiments, it hampers the analysis of the results that they obtained. This difficulty however disappears with the new experimental techniques used, for example, in Saleh et al. (1993), Tachie et al. (2004), and Goharzadeh et al. (2005). Indeed, in these experiments, there is no divider plate. The velocity profiles are measured in the whole domain using particle image velocimetry. An interesting point would be to compare these more details experiments to the results presented in this paper.

## 5 Conclusion

In this work, we analyze the jump conditions that must be imposed at a fluid/porous interface in order to account for the transfers that occur in the interfacial region. This general analysis is based on two up-scaling steps. The first one allows to obtain a continuous description of the problem. The transfers in the interfacial region are modeled via effective properties that vary in the interfacial transition regions. In this study, these effective properties are determined by filtering numerical simulations at the pore scale. Then, a second up-scaling step is performed. The physical features, which are not (or not correctly) accounted for by the macroscopic model, compared to the mesoscopic one, in the interfacial region, are assigned to the interface through jump conditions that involve excess quantities. These excess quantities depend on the interface location. But this dependence compensates the fact that the macroscopic models are different in the two homogeneous regions and that changing the interface location modifies the zone of influence of a given macroscopic model. For both the heat conduction and the Poiseuille flow problems, the macroscopic solutions are equivalent to their corresponding mesoscopic solutions whatever the position of the interface inside the transition region.

Finally, the Beavers and Joseph's slip boundary condition is analyzed. We show that by studying the transfers at a fluid/porous interface using a multi-scale approach, it is possible to recover the Beavers and Joseph's slip boundary condition. In this study, the conditions under which the Beavers and Joseph's relation is recovered are made explicit: (i) the transfers at the mesoscopic scale must satisfy Eq. 10 and (ii) the value of  $\sigma$  must be sufficiently large or the pressure and viscous surface-excess forces must vanish exactly at the same location. In both cases,  $\alpha = \sqrt{\phi_p}$  and the interface must be located at  $y_M = y_{fi}$  which is the center

of gravity of the friction surface-excess force. Thus, the difficulty is not to determine  $\alpha$ , but to determine  $y_{fr}$ . This can be done using our multi-scale approach. Furthermore, the sensitivity of the Beavers and Joseph's relation on the precise location of the interface inside the transition region has been illustrated.

## References

- Anderson, D.M., McFadden, G.B., Wheeler, A.A.: Diffuse-interface methods in fluid mechanics. *Annu. Rev. Fluid Mech.* **30**, 139–165 (1999)
- Beavers, G., Joseph, D.: Boundary conditions at a naturally permeable wall. *J. Fluid Mech.* **30**, 197–207 (1967)
- Beavers, G.S., Sparrow, E.M., Masha, B.A.: Boundary conditions at a porous surface which bounds a fluid flow. *AIChE J.* **20**, 596–597 (1974)
- Breugem, W.-P., Boersma, B.J., Uittenbogaard, R.E.: Direct numerical simulation of plane channel flow over a 3D cartesian grid of cubes. In: Reis, A.H., Miguel, A. (eds.) *Proceedings of the Second International Conference on Applications of Porous Media*, pp. 27–35. Evora Geophysics Center, Portugal (2004)
- Breugem, W.-P., Boersma, B.J., Uittenbogaard, R.E.: The laminar boundary layer over a permeable wall. *Transp. Porous Media* **59**(3), 267–300 (2005)
- Chandesris, M., Jamet, D.: Boundary conditions at a planar fluid-porous interface for a Poiseuille flow. *Int. J. Heat Mass Transf.* **49**(13–14), 2137–2150 (2006)
- Chandesris, M., Jamet, D.: Boundary conditions at a fluid-porous interface: An a priori estimation of the stress jump coefficients. *Int. J. Heat Mass Transf.* **50**(17–18), 3422–3436 (2007)
- Edwards, D.A., Brenner, H., Wasan, D.T.: *Interfacial Transport Processes and Rheology*. Butterworth-Heinemann, Boston, MA (1991)
- Emmerich, H.: *The Diffuse Interface Approach in Materials Science*. Springer, Berlin (2003)
- Goharzadeh, A., Khalili, A., Jorgensen, B.B.: Transition layer thickness at a fluid-porous interface. *Phys. Fluids* **17**, 057102 (2005)
- James, D.F., Davis, A.M.: Flow at the interface of a model fibrous porous medium. *J. Fluid Mech.* **426**, 47–72 (2001)
- Jamet, D., Chandesris, M.: On the intrinsic nature of jump coefficients at the interface between a porous medium and a free fluid region. *Int. J. Heat Mass Transf.* In Press, Available online (2008)
- Kaviany, M.: *Principles of Heat Transfer in Porous Media*. 2nd edn. Springer-Verlag, New York (1995)
- Kuznetsov, A.V.: Influence of the stress jump condition at the porous-medium/clear fluid interface on a flow at a porous wall. *Int. Commun. Heat Mass Transf.* **24**(3), 401–410 (1997)
- Larson, R.E., Higdon, J.J.L.: Microscopic flow near the surface of a two-dimensional porous media. Part 1. Axial flow. *J. Fluid Mech.* **166**, 449–472 (1986)
- Larson, R.E., Higdon, J.J.L.: Microscopic flow near the surface of a two-dimensional porous media. Part 2. Transverse flow. *J. Fluid Mech.* **178**, 119–136 (1987)
- Nozad, I., Carbonell, R.G., Whitaker, S.: Heat conduction in multiphase systems I: Theory and experiment for two-phase systems. *Chem. Eng. Sci.* **40**, 843–855 (1985)
- Ochoa-Tapia, J.A., Whitaker, S.: Momentum transfer at the boundary between a porous medium and a homogeneous fluid—I. Theoretical development. *Int. J. Heat Mass Transf.* **38**(14), 2635–2646 (1995)
- Quintard, M., Whitaker, S.: Transport in ordered and disordered porous media—II. Generalized volume averaging. *Transp. Porous Media* **14**, 179–206 (1994)
- Saffman, P.G.: On the boundary condition at the surface of a porous medium. *Stud. Appl. Math.* **L**(2), 93–101 (1971)
- Sahraoui, M., Kaviany, M.: Slip and no-slip velocity boundary conditions at interface of porous, plain media. *Int. J. Heat Mass Transf.* **35**(4), 927–943 (1992)
- Saleh, S., Thovet, J.F., Adler, P.M.: Flow along porous media by partial image velocimetry. *AIChE J.* **39**(11), 1765–1776 (1993)
- Tachie, M.F., James, D.F., Currie, I.G.: Slow flow through a brush. *Phys. Fluids* **16**(2), 445–451 (2004)
- Taylor, G.I.: A model for the boundary condition of a porous material. Part I. *J. Fluid Mech.* **49**(2), 319–326 (1971)
- Valdès-Parada, F.J., Goyeau, B., Ochoa-Tapia, J.A.: Diffusive mass transfer between a microporous medium and an homogeneous fluid: Jump boundary conditions. *Chem. Eng. Sci.* **61**(5), 1692–1704 (2006)
- Valdès-Parada, F.J., Goyeau, B., Ochoa-Tapia, J.A.: Heat conduction with chemical reaction in three-phase systems: Effective medium equations and jump boundary conditions. In: *Eurotherm Seminar No. 81 Reactive Heat Transfer in Porous Media*, Ecole des Mines d'Albi, France, 4 June 2007a

- Valdès-Parada, F.J., Goyeau, B., Ochoa-Tapia, J.A.: Jump momentum boundary condition at a fluid-porous dividing surface: Derivation of the closure problem. *Chem. Eng. Sci.* **62**, 4025–4039 (2007b)
- Whitaker, S.: The species mass jump condition at a singular surface. *Chem. Eng. Sci.* **47**(7), 1677–1685 (1992)
- Whitaker, S.: *The Method of Volume Averaging*. Kluwer Academic Publishers, The Netherlands (1999)